Article

Not peer-reviewed version

Time and Spatially Resolved Operando Small-Angle X-ray Scattering Measurements during Injection Moulding of Plastics

Geoffrey R. Mitchell * , Matteo Arioli , Anabela Pavia Massano , Daniel Pedra Da Silva , Fabio A. Gameiro , Pedro Carreira , Marc Malfois , Joao Matias , Paula Christina Pascoal-Faria , Artur Mateus

Posted Date: 15 August 2023

doi: 10.20944/preprints202308.1135.v1

Keywords: injection moulding; small-angle X-ray scattering; morphology; isotactic polypropylene

Article

Time and Spatially Resolved Operando Small-Angle X-ray Scattering Measurements During Injection Moulding of Plastics

Matteo Arioli [1], Anabela P. Massano [2], Daniel P. da Silva [2], Fábio Gameiro [2], Pedro Carreira [2], Marc Malfois [3], João Matias [2] , Paula Pascoal-Faria [2], Artur Mateus [2] and Geoffrey R. Mitchell [2,*]

[1] Departament d'Enginyeria Química, Universitat Politècnica de Catalunya, Av. Eduard Maristany 10-14, 08019 Barcelona, Spain MA matteo.arioli@upc.edu

[2] Centre for Rapid and Sustainable Product Development, Polytechnic of Leiria, 2430-080 Marinha Grande, Portugal. APM anabela.p.massano@ipleiria.pt, DPS daniel.silva@ipleiria.pt, FG fabio.a.gamerio@ipleiria.pt, PC pedro.carriera@ipleiria.pt, JM joao.matias@ipleiria.pt PPF paula.faria@ipleiria.pt, AM artur.mateus@ipleiria.pt, GRM geoffrey.mitchell@ipleiria.pt

[3] NCD-SWEET Beamline, ALBA Synchrotron Light Source, Cerdanyola del Vallès, Barcelona, Spain

* Correspondence: geoffrey.mitchell@ipleiria.pt; Tel.: +251 962426 925

Abstract: We have recently introduced the possibility of performing operando small-angle X-ray scattering measurements using a novel industrially relevant injection moulding system for plastics. We show that useful time-resolving measurements can be performed with a time-cycle of 1s and we highlight the possible steps to reduce this to 0.5s. We show how we can use the transmission measurements to provide a time-marker when plastic first enters the mould cavity in the region probed by the incident X-ray beam. We show the opportunities provided by this experimental stage mounted on the NCD-SWEET beamline at ALBA to probe the reproducibility of the injection moulding system on different scales. The design of the equipment allows the development of the structure and the morphology to be evaluated in different parts of mould cavity and we evaluate any differences in a rectangular mould cavity. We identify future prospects for this equipment in terms of novel mould heating and cooling systems and the opportunities for quantitatively evaluating radical approaches to injection moulding technology.

Keywords: injection moulding; small-angle X-ray scattering; morphology; isotactic polypropylene

1. Introduction

Injection moulding is the most widely used technology for the manufacturing of plastic parts [1]. The process is usually completely automated for the repeatable and reproducible production of parts that in general need no finishing. The first injection moulding machine was patented by the Hyatt brothers, John and Isaiah in 1872 [2]. These first machines were quite primitive in comparison to contemporary systems. The technology was revitalized in the 1940s by the replacement of the plunger to inject the hot plastic in to the mould by an extrusion screw [3]. The rotating screw gave the machine better control over the injection speed and consequently improved the quality of the plastic parts produced. The screw also allowed mixing of, for example, recycled materials with virgin materials due to the mixing action of the screw. The interaction of the screw with the solid pellet feed stock greatly contributes to the first stage process of melting or softening the plastic due to friction. The remaining heat comes from electrical band heaters. Screw machines now make up the vast majority of all injection moulding machines. Not long after the introduction of the screw extrusion injection mouding system, new high-quality thermoplastics including polyethylene, polypropylene, polystyrene and nylons became available [4] and greatly helped the acceleration in the adoption of injection moulding of plastics as a manufacturing technology.

Injection moulding of plastics is a deceptively simple technology. Plastic feed stock usually in the form of mm sized pellets is heated in to the liquid state and then injected at high pressure in to a metallic mould to define the shape. The plastic cools and becomes solid after passing through a glass

transition or crystallising to form a semi-crystalline solid. The solid part is then ejected from the mould. This work is focused on semi-crystalline polymers such as isotactic polypropylene, polyethylene, nylon and some biobased plastics such as polyhydroxybutyrate and polybutylene succinate. In these materials, the flow processes inherent to injection moulding and the rapid changes of temperature involved as the fluid plastics enters the mould have a profound impact on the structure and morphology which develops as the plastic solidifies and therefore on the properties of the part [5]. Previous reports in the literature have focused on the post-processing characterisation of injection moulded parts and attempts have been made to reconstruct the history of the development of the structure and morphology during the injection moulding cycles [6,7]. There are a few exceptions to this, including experimental stages which approach industrial processing conditions. One of the earliest in-situ scattering studies was focused on Reaction Injection Moulding. This is a low-pressure process in which a reactive mixture is injected at low pressure in to a mould cavity. The low pressure used means that a variety of materials can be used to fabricate the mould. Elwell et al [8-9] used time-resolved small-angle X-ray scattering to study the microphase separation which takes place during the formation of the solid foam. Mateus et al [10] used time-resolved scattering small-angle X-ray scattering to evaluate the microphase separation and showed that the rate of reaction of the components was slower that the time scale of forming the morphology. In Hamburg, Zachmanns group [11] working on beamline A1 at HASYLAB were amongst the first to develop what can be seen as a realistic industrial manufacturing process, exploring fibre spinning. A more recent development involved polymer films which are blown using air pressure on extruded tubular films. This is a widely used process although it is a complex process with fast changing temperatures and different deformation geometries. Van Drongelen et al [12] were probably the first to explore the film blowing process using time-resolving wide-angle X-ray scattering techniques. A limitation of this approach is that the preferred orientation of the chain folded-lamellar crystals is more difficult to evaluate using WAXS and later work included small-angle X-ray scattering measurements [13]. Zhang et al [14] mounted a film blowing system on a SAXS beamline [15] to evaluate polyethylene films prepared in this manner, and used operando scattering to explore by adjusting the height of the extruder die with relationship to the incident beam. It was possible to evaluate different parts of the blown film at defined distances from the extruder die. The authors highlight how they were able to follow the network formation from the entangled melt through the formation of crystalline network points obtaining quantitative data which is able to inform on computational models of film blowing and the dependence of the process on the molecular parameters. Most other work reported more fell in to the realm of scientific studies but some recent work from Liao et al [16] developed an operando X-ray scattering system for injection moulding using a metallic mould and diamonds as X-ray transparent windows. They used this system in conjunction with intense flux at the synchrotron beam-time BL19U2 [13] at the Shanghai synchrotron radiation facility to determine the characteristics of the shish-kebab structures that are created during crystallization in he the micro-injection moulding. However, in the last year, a new major project at CDRSP has developed an industrially relevant injection moulding system which can be mounted on the NCD-SWEET beam at the ALBA Synchrotron light source to perform operando small-angle X-ray scattering measurements [17]. X-ray scattering is a powerful tool for operando experiments. The bright sources of X-rays available via an undulator at a Synchrotron Light Source enable effective time-resolving measurements [18]. The analysis of the data is largely unambiguous as the theory of X-ray diffraction physics is well understood and well developed and the optimum sample thickness of 1 - 2 mm is a practical industrial scale [19]. Moreover, the samples need not be optically clear and can contain pigments and other nanofillers. Small-angle scattering which covers the important scale of ~10nm and provides critical information on the formation and the preferred orientation of chain folded lamellar crystals which are particularly important in determining the properties of the final part [20].

The injection moulding system used in this work is designed and fabricated using industry standard materials and protocols, so that information gained in this work can be directly translated to industrial practice. The current work focuses on what can be achieved in terms of time and spatially resolved measurements using this new injection moulding system and the NCD-SWEET

Preprints (www.preprints.org) | NOT PEER-REVIEWED | Posted: 15 August 2023 doi:10.20944/preprints202308.1135.v1

SAXS/WAXS beamline at the ALBA Synchrotron Light Source and the prospects for future developments and experimental work.

2. Materials and Methods

This work is only possible due to the developments at third generation synchrotron light sources such as ALBA and the provision of bright energy tuneable sources of hard X-rays [18].

Figure 1 shows a schematic representation of the NCD-SWEET beamline at ALBA [18]. 3GeV electrons moving at speeds close to the speed of light pass through the undulator where they are further accelerated by arrays of Samarium Cobalt magnets. The static magnetic field alternates along the length of the undulator with a wavelength λ_u, which for the NCD-SWEET undulator is 21.6mm with 92 periods. Electrons which traverse this periodic magnet structure are driven to undergo oscillations and radiate energy. The radiation produced in an undulator is particularly intense and is concentrated in narrow energy bands [22]. It is also highly collimated in the orbit plane of the electrons. The radiation produced in this way enters the beamline. The undulator is a harmonic device and on the NCD-SWEET beamline the first harmonic is the most intense. The energy is rather low at 2keV and instead we utilize the 7th harmonic which has an energy of 12.4keV corresponding to a wavelength of 1Å which offers a greater transmission through the aluminium windows. This choice of wavelength is a trade-off between the intensity of the harmonic produced in the undulator and its absorption by the aluminium alloy in the mould insert windows.

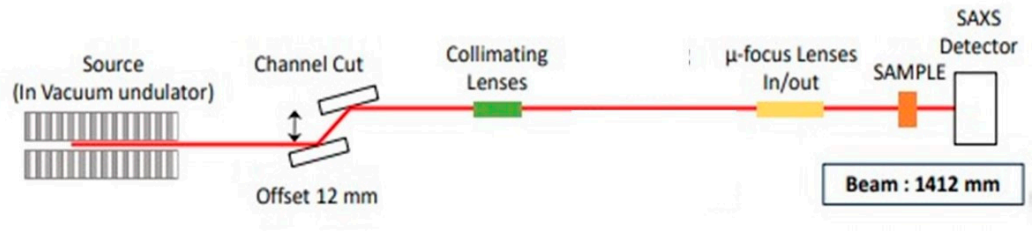

Figure 1. A schematic of the NCD-SWEET beamline at the ALBA synchrotron light source [18].

The injection moulding unit follows a conventional design with the mould cavity prepared using standard mould plates and mould inserts in an aluminium -silicon alloy AW6082 [23]. At automatic mechanism for opening and closing the mould cavity is provided using a rail structure. For the injection process, an Industrial Autonomous Injection Unit, UAI6/1OP, from the Rambaldi Group is mounted above the mould. This is an autonomous unit and the injection is all hydraulic [24]. The unit is fitted with a Euromap connection which makes the additional other components or the interface to the ALBA Synchrotron controls, very straightforward. Figure 2a shows the system showing the entry points of the incident X-ray beam, Figure 2c shows the exit ports and Figure 2b the assembled system viewed from the side. The mould inserts have been machined with 6 cylindrical holes which stop ~ 0.08mm from the far side, so as to provide a "window" which will enable the X-ray beam to pass through without excessive absorption, the transmission is measured at ~ 70%, but this thickness is sufficient to withstand the high pressure in the cavity during the injection phase. The system is described in detail elsewhere [17,25]. The whole system is mounted on a motorized translation stage which enable the system to be position so that the incident X-ray beam can pass through any of the 6 windows.

Preprints (www.preprints.org) | NOT PEER-REVIEWED | Posted: 15 August 2023 doi:10.20944/preprints202308.1135.v1

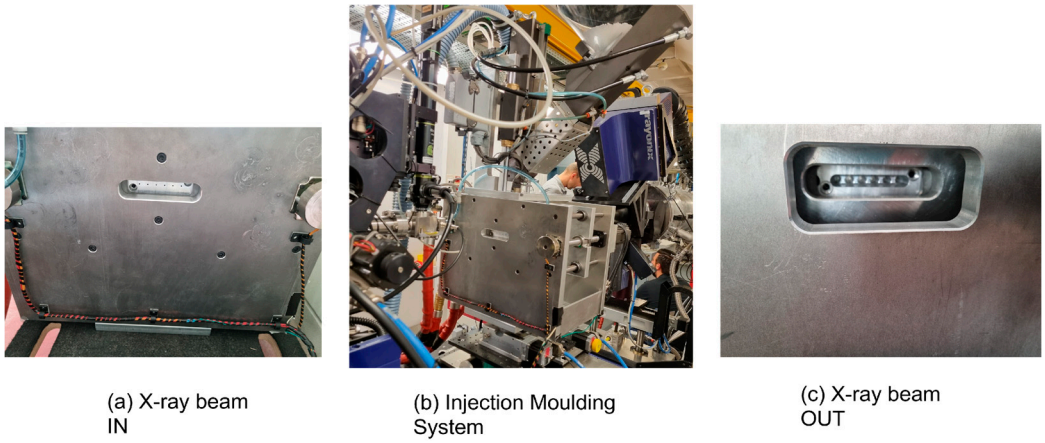

Figure 2. Operando Injection Moulding System.

The beamline is fitted with a 2D detector, a DECTRIS Pilatus3S 1 M detector, to record the small-angle X-ray scattering patterns and this was mounted 6.7m away from the mould cavity. This enabled SAXS patterns to be recorded over a scattering vector $|\underline{Q}|$ range from 0.002 $Å^{-1}$ to 0.125 $Å^{-1}$ where $|\underline{Q}| = 4\pi \, Sin\theta/\lambda$, 2θ is the scattering angle and λ is the incident wavelength which was 1Å. The beamline in terms of sample to detector distance was calibrated using the well-known calibrant sodium behenate. To minimize the effects of scattering by the air, the space between the mould cavity and the detector is fitted with a vacuum tube. To prevent the intense forward beam reaching and saturating the detector it is fitted with a small absorbing beam stop. This also contains a photodiode which can be used to make transmission measurements. Just before the sample, a ion-chamber is mounted so that the incident intensity of the X-ray beam can be measured. The ALBA Synchrotron Light Source, in common with most other 3rd generation synchrotron rings, has an automatic system to top-up the ring current every twenty minutes, so as to maintain a more or less constant current. In the intervening periods, the ring current and hence the intensity of the X-ray beam from the undulator will decay slowly and then increase at each top up. An example of this is shown in Figure 3. To account for this small variation, the measured small-angle X-ray scattering data can be normalized to the measured incident beam intensity, but otherwise it is a constant output source.

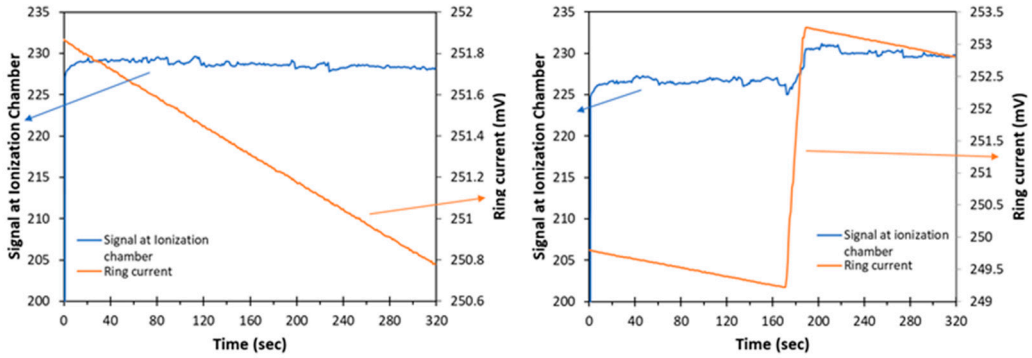

Figure 3. Variation of the storage ring current (orange) and the Ionization Chamber signal (blue) during decaying operations (left) and in the topping-up moments (right). The sudden increase in the signals in the first second is associated to the aperture of the fast shutter.

The work described here was performed using some standard industrial grades of isotactic polypropylene. Table 1 shows the acronym for each grade and the reported Melt Flow Index and any additives incorporated in this grade.

Table 1. The grades of isotactic polypropylene used in this work

Preprints (www.preprints.org) | NOT PEER-REVIEWED | Posted: 15 August 2023 doi:10.20944/preprints202308.1135.v1

Acronym	Manufacturer	Grade	MFI g/10 mins at 230C	Notes
PP1	Lyndon Basel	MOPLEN HP 500N	12	General purpose suitable for food contact applications.
PP2	Repsol	ISPLEN PR595C2M	45	Phthalate free random copolymer which is clarified and contains antistatic additives.
PP3	SABIC	595A	47	Designed for Automotive applications.

3. Results

A key feature of the process of injection moulding is the high level of reproducibility that makes the technology particularly suited to mass production. This in essence relates to the external shape and the surface finish. These multiscale experiments enable us to probe to what length scale injection moulding is reproducible. This is not to say that the positions and conformations of the molecules in two successive moulded parts are exactly the same. Rather we need to check if the characteristics of the structure and the morphology are similar.

3.1. Basic Observations

Figure 4a shows a small-angle X-ray scattering pattern for PP1 recorded during 1s following plastic first entering the mould cavity. The injection temperature is 230 °C and the mould temperature is 50 °C. The flow axis of the plastic in the mould cavity is horizontal, the intense scattering feature in the centre of the pattern largely arises from the scattering from the aluminium alloy which forms the "window" in the mould. In the very centre of the pattern there is black circular object which is the beam stop which is placed to intercept the intense forward going beam which has passed through sample. The sample volume here is small and only part of the material in the mould cavity is crystalline. As a consequence, the scattering intensity is weak and is difficult to visualise against the strong scattering from the window, Figure 4b shows the same pattern with the background scattering from the empty mould cavity, subtracted from Figure 4a. The remaining scattering is typical for a chain folded lamellar crystal stack structure. In other words, this scattering is from the first crystals to form in the mould cavity after the plastic has been injected. The slightly higher intensity along the flow axis direction to the left and right of the centre of the zero angle of the pattern is indicative of a certain level of preferred orientation of the crystals.

Preprints (www.preprints.org) | NOT PEER-REVIEWED | Posted: 15 August 2023 doi:10.20944/preprints202308.1135.v1

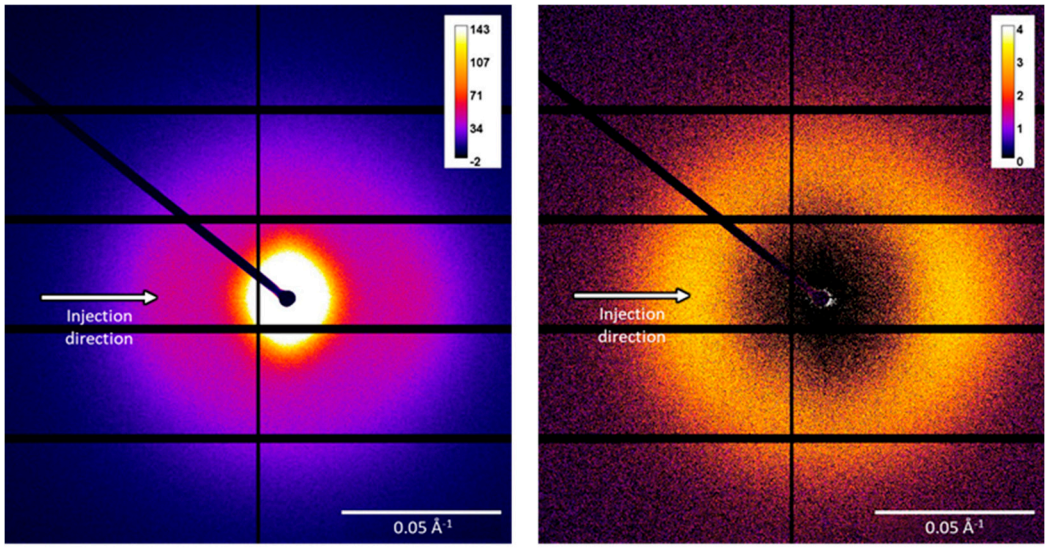

Figure 4. (a) left, original SAXS pattern acquired during 1 second, (b) right the same pattern as before, in which the image collected for an empty mould cavity was subtracted as background.

Figure 5 shows the integrated intensity in the image shown in Figure 4b as a function of the scattering vector |Q|. This shows an intensity curve typical of the SAXS data from a semicrystalline polymer. The broad peak centered around a |Q| of 0.043 $Å^{-1}$ arises from the contrast between the chain folded lamellar crystals and the intervening amorphous material which exhibits a lower density. From the data shown in Figure 5 we can obtain a value for the so-called long period Lp which is the sum of the lamellar thickness and the thickness of the intervening amorphous material, here the peak position indicates a value for the long period of 146 Å. From the azimuthal variation of the intensity at a fixed value of |Q|, we can evaluate a measure of the level of preferred orientation.

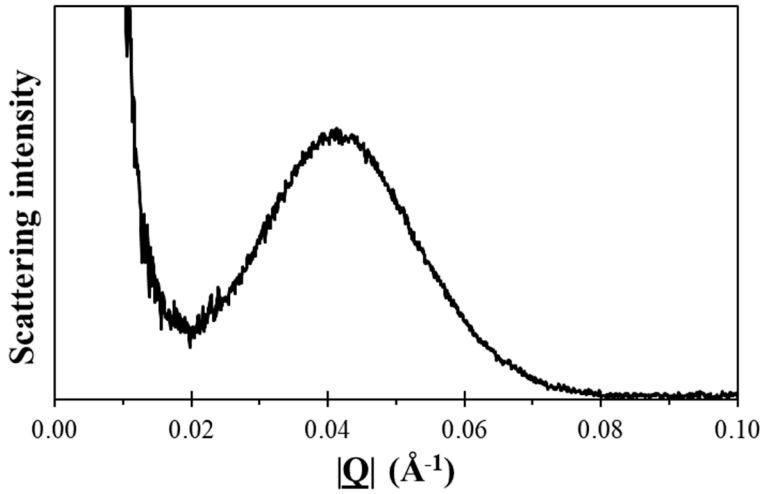

Figure 5. Azimuthal integration of a SAXS patterns present in Figure 4.

Figure 6 shows the value of the photodiode mounted inside the beamstop and its variation with time. When plastic material enters the mould cavity the value of this signal is reduced due to absorption of the beam by the plastic material and it provides a timing marker to unify the timescales. The value of the transmission signal, I_t, is related to the incident beam I_0 through the following equation

$$I_t = I_0 \exp(-At) \quad (1)$$

Preprints (www.preprints.org) | NOT PEER-REVIEWED | Posted: 15 August 2023 doi:10.20944/preprints202308.1135.v1

where A is the linear absorption coefficent, which depends on the elemental composition of the plastic and t is the thickness of the plastic in the mould cavity. From this we can see that $\ln(I_t/I_0)$ is linearly related to the thickness. In Figure 6 we have also plotted the intensity of equivalent peak height of the "long period" peak shown in Figure 5 for successive time-resolved images. This peak arises from the scattering from alternating lamellar crystals and a region of non-crystalline polymer and as a consequence it will reach a maximum at 50% V/V of lamellar crystals. A further complication is that as the temperature of the of the plastic cools, the difference in density between the lamellar crystals and the amorphous polymer narrows, and hence the scattering intensity reduces as can be observed in Figure 6.

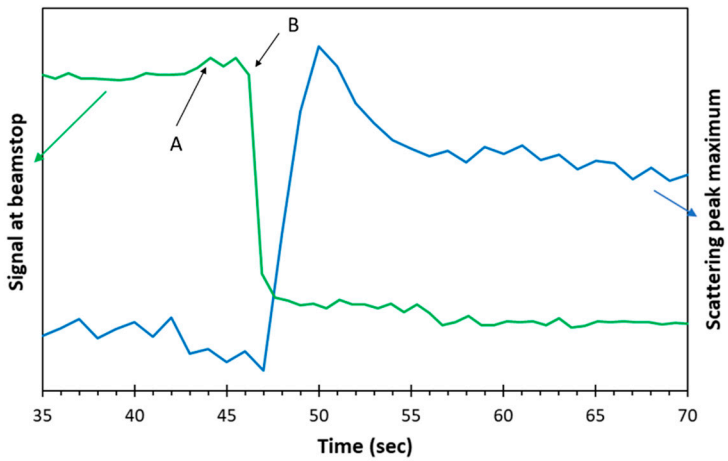

Figure 6. Signal of transmitted radiation intesity collected at the beamstop photodiode. Are visible the injection point (A) and the moment in which polymer enters in the mould (B)

3.2. Reproducibility

The major advantage of injection moulding as a manufacturing technology is its ability to produce large numbers of identical parts with the same surface finish, without requiring extensive post-processing. In this section we explore whether this level of reproducibility extends to the structure and morphology of the part. By this we mean that we will explore whether the characteristics of the time development of the structure and morphology are equivalent in repeated parts, rather than whether the molecular organization is identical at an atomic level. Figure 7 shows time sequences of SAXS patterns recorded during an injection moulding cycle for PP1, the first image is for the empty mould cavity, the time resolution here is more or less a second between successive images, time runs horizontally .

Preprints (www.preprints.org) | NOT PEER-REVIEWED | Posted: 15 August 2023 doi:10.20944/preprints202308.1135.v1

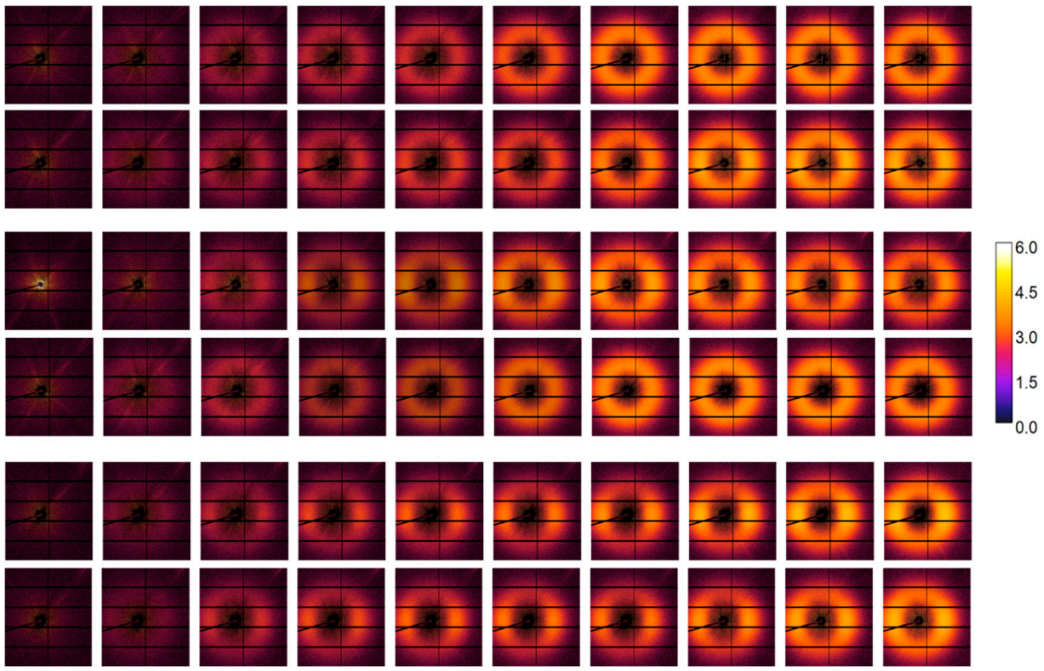

Figure 7. Sequences of 1 second acquisition scans, correspondent to the monitoring of the first window. 1st and 2nd lines: Injection Temperature = 250 °C, 3rd and 4th lines: Injection Temperature = 230 °C, 5th and 6th lines: Injection Temperature = 210 °C.

The time sequences are in pairs, the top two are for an injection temperature of 250 °C, the middle pair is for 230 °C and the lowest pair is for 210 °C. We can observe two trends looking at these images. The first is that the emergence of the crystalline pattern is slower at 250 °C than at 210 °C and the second is that at lower injection temperatures there is a distinct level of preferred orientation in the patterns as there is a great intensity in the horizontal section compared to the vertical section of the rings. This latter trend can be associated with the shorter time between the flow and the subsequent nucleation of crystals. This shorter time will mean that the longest chains extended in the flow will not have relaxed by the time crystal growth of the matrix begins. We also show in Figure 9, plots of the transmission versus time and the height of the peak in the integrated plot (see section 3.1).

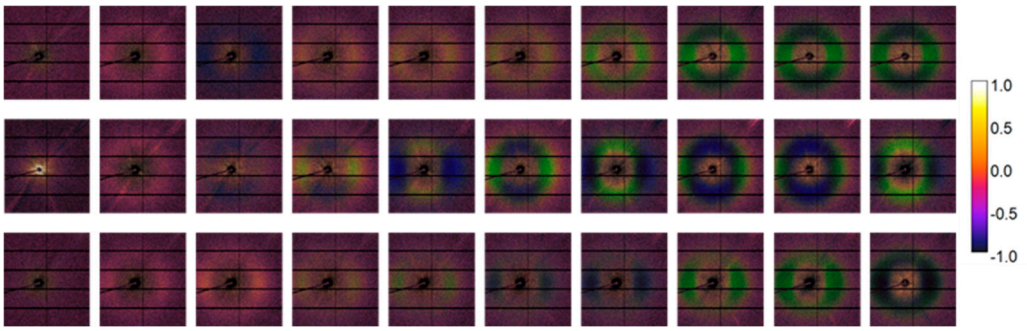

Figure 8. Images showing maps of χ^2 calculated as described in the text for pairs of time equivalent images for the three temperatures shown in Figure 7. Time runs horizontally with ~1s between adjacent images. The false colour mapping of the intensity has been adjusted to maximise the the visualisation of these small differences.

Preprints (www.preprints.org) | NOT PEER-REVIEWED | Posted: 15 August 2023 doi:10.20944/preprints202308.1135.v1

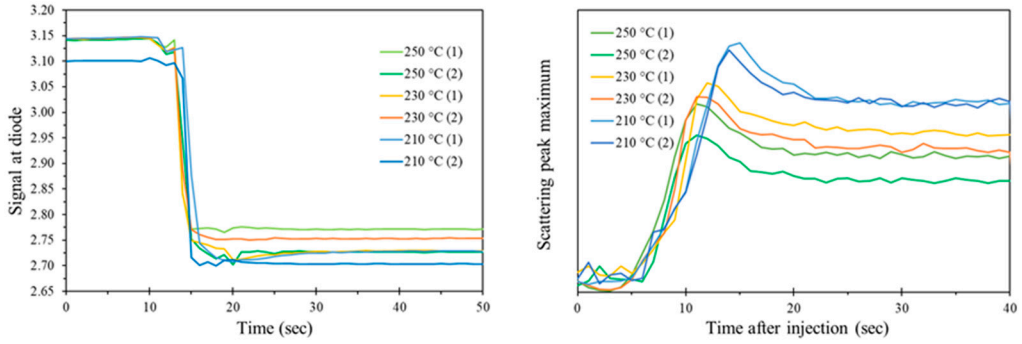

Figure 9. Left: Intensity signal at photodiode for the different injection at the different indicated temperatures. Right: scattering peak maximum variation with time after the injection for the different injections.

A visual inspection of the pairs of time-equivalent SAXS patterns in Figure 7 for the three different experimental temperatures shows that time-sequence of the development of the SAXS patterns is the same for repeated runs. We have calculated the χ^2 parameter for each pixel in essentially time-equivalent pairs using the following equation:

$$\chi^2 = \frac{(I_{px1} - I_{px2})^2}{\sigma^2} \quad (2)$$

where I_{px1} and I_{px2} represent the intensity of the same pixel in images 1 or 2, respectively and σis the standard deviation of the first point. As the Pilatus detector is a photon counting system, the standard deviation is given by $(I_{px1})^{0.5}$. We have plotted the value of $\sum\chi^2$ /n, where n is the total number of pixels in the image, for each difference image shown in Figure 8 for each of the three experimental temperatures as a function of time and the total value of χ^2 for each image are shown in Figure 10. Inspection of the curves in Figure 10 confirms the reproducibility of the successive time-resolving sequences. We can see that when crystallisation is initiated at all temperatures but particularly at the lower temperatures, the values of χ^2 rises slightly, as the images are changing more rapidly with time, the small errors in time equivalence between images are more significant.

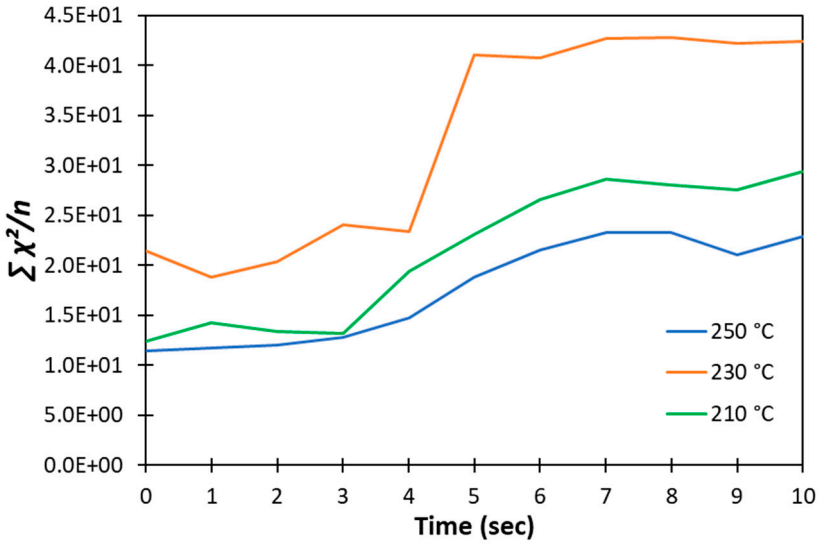

Figure 10. Total χ^2/n values for the three experimental runs at the three extrusion temperatures shown in Figure 8.

3.3. Spatial variations

The constraints on the design of the mould cavity limits sampling the SAXS data to one of six predetermined positions, corresponding to the positions in the mould insert where the mould

Preprints (www.preprints.org) | NOT PEER-REVIEWED | Posted: 15 August 2023 doi:10.20944/preprints202308.1135.v1

material has been thinned sufficiently to allow adequate transmission of the incident and scattered beams through the mould inserts. Now of course, the challenge of predetermined positions is that they may not be the ideal position for extracting data or comparing to the predictions of a simulation. We emphasise here that it is straightforward to fabricate an alternative mould insert with optimised positions and install in the injection moulding system. Here we report on measurements made using the standard mould insert in which 6 windows are distributed evenly along the central line of the mould with a standard spacing of 11mm. Figure 11 shows the time-resolved sequences of SAXS data for the first four windows of the mould. Each time sequence starts before the plastic enters the mould cavity. Figure 12 shows the accompanying 1D plots for the time markers and the intensity of the equivalent peak to that shown in Figure 5 but for the images shown in Figure 11 as a function of time.

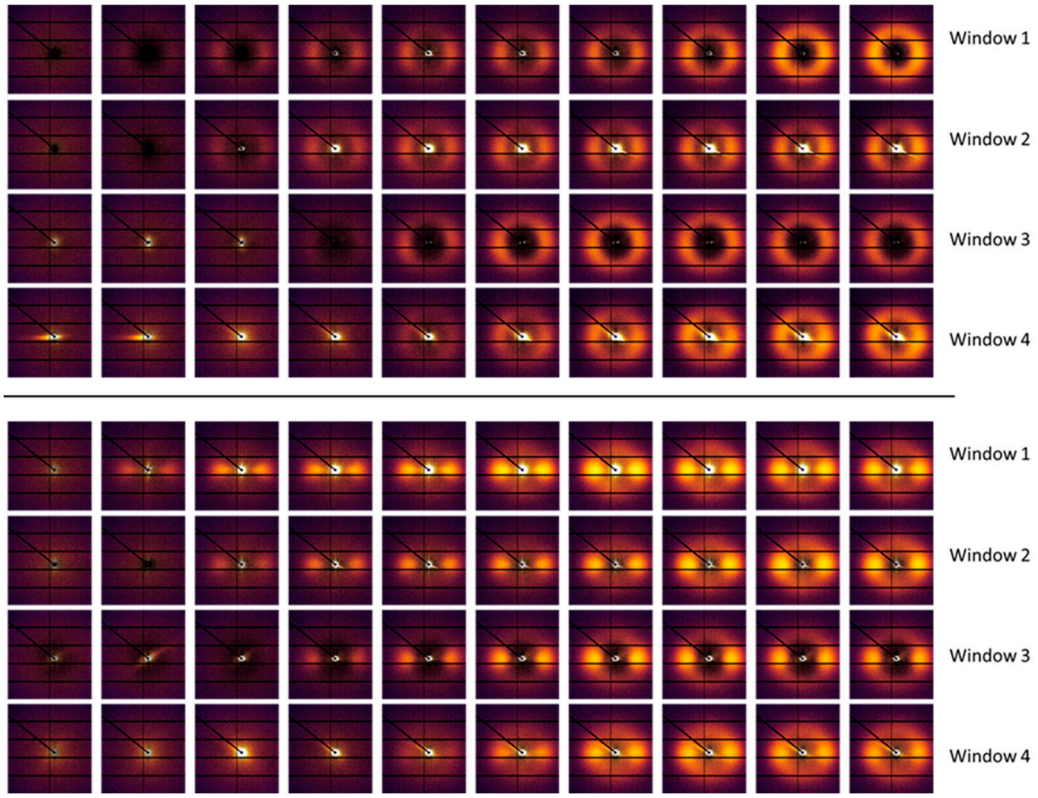

Figure 11. Time resolved sequences of SAXS patterns obtained by monitoring the first 4 windows of the mould. On top, the patterns related to PP1, while at the bottom, related to PP2. Time proceeds from left to right. The flow direction of the plastic is horizontal.

It can be seen from Figure 11 that the entry of the plastic in to the area of mould cavity in line with the windows is delayed by ~1s from window 1 to window 2 and so on to window 4. The consequence of this is that the development of crystallinity in that material is also delayed from windows 2,3 and 4 as can be seen in Figure 12. We can also notice that the time sequences for windows 2, 3 and 4 is similar to that for window 1. Figure 12 shows that the development of crystallinity in the relevant parts of the mould cavity varies from window 1 to window 4. We speculate that it is related to a reduction in the temperature of the molten plastic as it moves along the length of the mould cavity. In future work we will consider the value of extending the length of the mould cavity in order to enhance this possible effect.

Preprints (www.preprints.org) | NOT PEER-REVIEWED | Posted: 15 August 2023 doi:10.20944/preprints202308.1135.v1

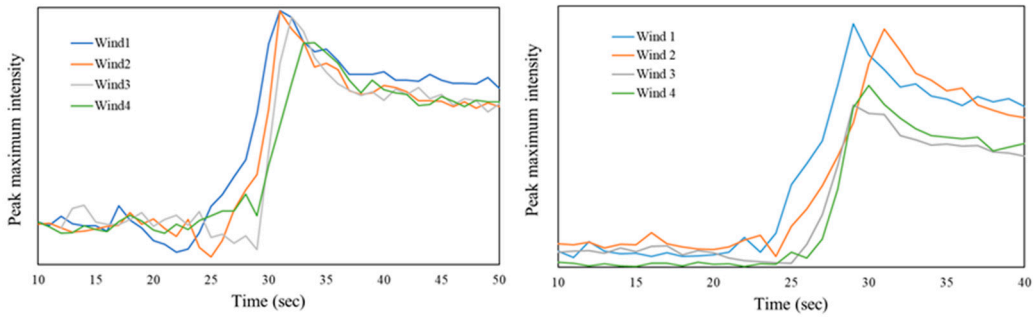

Figure 12. Scattering peak maximum intensity variation towards time for the PP1 (left) and PP2 (right).

3.4. Time variation

The preceding sections have demonstrated the data which are available in these operando X-ray scattering measurements of injection moulding. The availability of digital data means that we can access more information by simple manipulations of the data. For example, Figure 13 shows the first two images in a time resolving time sequence for the injection moulding of PP2 with an extrusion temperature of 210 °C and a mould temperature of 50 °C. As with all of the data shown in this work each of the images is receiving the cumulative scattered intensity for the structure formed since the start of the moulding processing.

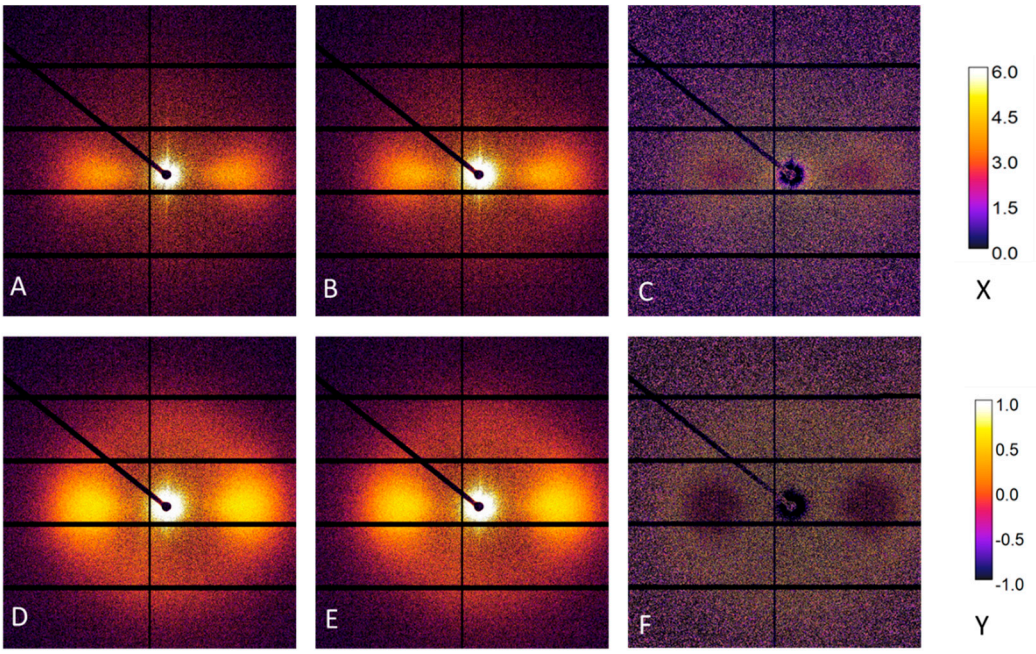

Figure 13. A, B: 1st and 2nd seconds of crystallization with their difference, depicted in C. D, E: 9th and 10th seconds of crystallization with their difference, showed in F. X represents the colour scale for A, B, D and E, while Y for C and F images (enlarged to enhance the readability). Clearly visible the fact that from 1st to 2nd the majority of the crystallization is oriented (highly anisotropic) while between 9th and 10th seconds, as seen in the peak maximum intensity, there is a modification in the structure towards a more isotropic structure (the "lobes" are darker while the "ring" is lighter)

The image shown in Figure 13B is that shown in Figure 13A plus the data recorded for the structure development in the second time interval. Now it is interesting to ask the question, does the crystallization that takes place in the 2nd second, the same as takes place in the first second. Figure 13C reveals the answer to this question and clearly the answer is yes. Although the additional level

Preprints (www.preprints.org) | NOT PEER-REVIEWED | Posted: 15 August 2023 doi:10.20944/preprints202308.1135.v1

of scattering is low we can see that the lobes of the lamellar stack scattering is essentially the same as in the first second in terms of azimuthually breadth. However, there is a small shift in the peak position, arising from a change in temperature. Now we can extend the questions to the 9th and 10th images. Even in this case, the idea that elaborates the characteristics as the same, can be supported. It is also possible, in this case, to distinguish between the formation of a second, more isotropic, structure, highlighted by the fact that a more visible scattering ring is forming around the lobes. This, again, confirms a change in the temperature in the cooling system, causing a different lamellar reorganization (see Figure 15). We emphasise the self-evident value of an even brighter sources, which will increase the signal/noise ratio in such difference images.

3.5. Preferred Crystal Orientation

The flow fields inherent in the process of injection moulding with plastics may lead to formation of a preferred orientation of the lamellar chain folded crystals. As we are dealing with lamellar crystals, we need to identify the vector to define the preferred orientation. Perhaps the most obvious is the vector normal to the fold surface of the chain folded crystal. This may, in some cases, present problems as the chain folded crystals are not always planar and as Keller et al. showed for some polyethylene samples the crystals may be twisted [26]. This is not the case here, but perhaps a more specific vector is the growth direction of the chain folded crystals. This is well defined by the crystallography of the crystals.

We can obtain information of the level of preferred orientation from the azmuthual variation in intensity I(α) at a constant value of $|\underline{Q}|$. In Figure 14 we show the azimuthal variation of the intensity of the lamellar crystal stack scattering (Figure 5b) for SAXS patterns recorded for the injection moulding of PP1 with an injection temperature of 210 °C and a mould temperature of 60 °C. for time equivalent images for the 4 window positions previously considered. α=0 is defined as parallel to the flow direction, which is horizontal in the SAXS patterns recorded in this work. Mitchell and co-workers have developed and used a robust mathematical methodology to evaluate the anisotropy from X-ray scattering data [27-29]. The basic method is encapsulated in the equation below

$$I_{2n}(|\underline{Q}|) = (4n+1)\int_0^{\pi/2} I\ (|\underline{Q}|,\alpha)P_{2n}(\cos\alpha)\sin\alpha.d\alpha \quad (3)$$

where $P_{2n}(\cos\alpha)$ are a series of Legendre Polynomials. In this work, only the even orders are required due to the inversion centre in the scattering pattern for a weakly absorbing sample, such as the hydrocarbon-based polymers used. Equation 3 identifies the fraction of the shape of the intensity $(I|\underline{Q}|,\alpha)$ in polar coordinates, with each of the harmonic functions shown in Figure 16 and then scaling that with the scattering for a perfectly aligned system.

$$< P_{2n}^{a}\cos(\alpha) >= \frac{I_{2n}^{a}(|\underline{Q}|)}{I_{0}^{a}(|\underline{Q}|)(4n+1)P_{2n}^{m}(\cos\alpha)} \quad (4)$$

where $P^{m}_{2n}(\cos\alpha)$ are the normalised amplitudes for the scattering of a perfectly aligned system. The data shown in Figure 14 shows a modest level of anisotropy for PP1 compared to the higher level of anisotropy exhibited by the data for PP2. In both cases the maximum scattering is observed at α=0°, and 180° indicating that the lamellar stack is arranged parallel to the flow direction , with the lamellar growth direction perpendicular to the flow direction as is expected for a system nucleated by row nuclei [30,21]

Preprints (www.preprints.org) | NOT PEER-REVIEWED | Posted: 15 August 2023 doi:10.20944/preprints202308.1135.v1

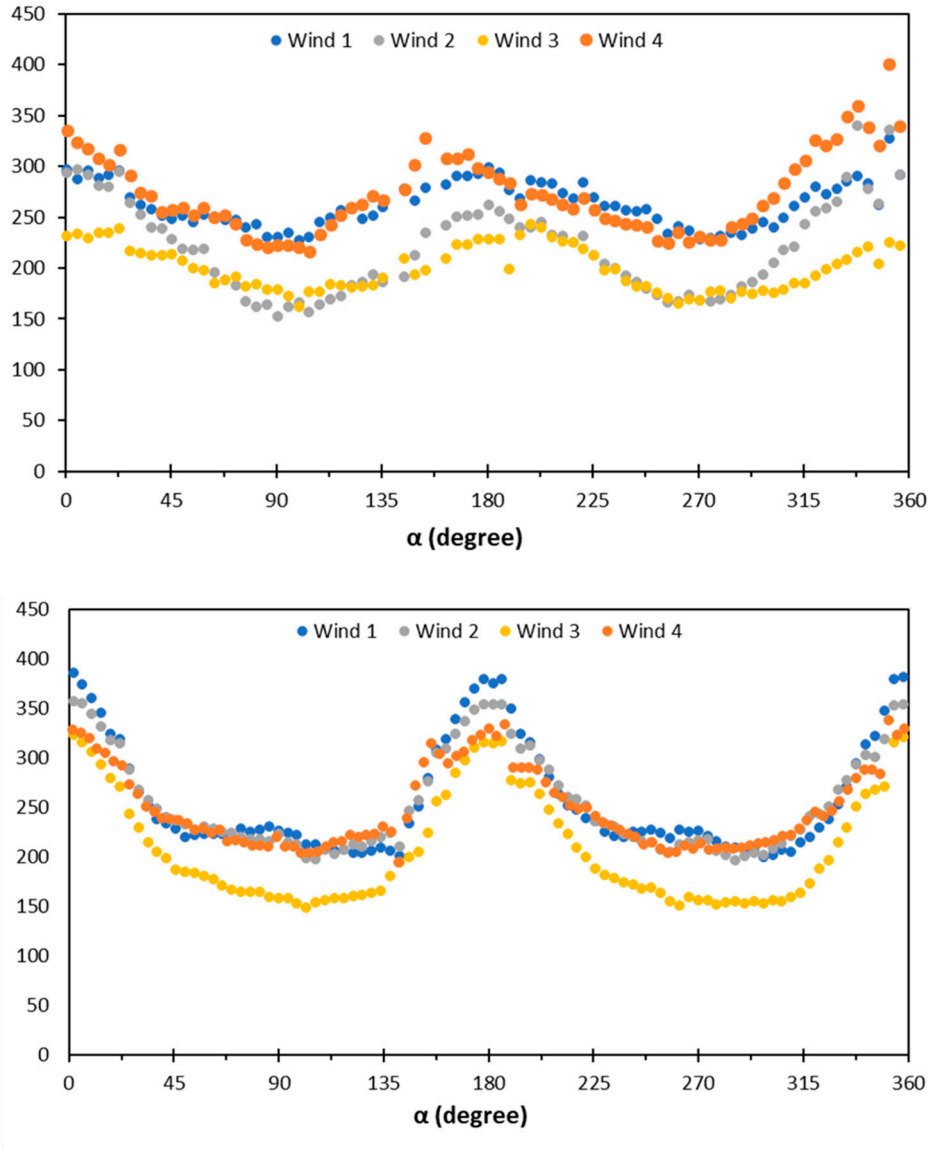

Figure 14. Azimuthual profiles for PP1 (top image) and PP2 (bottom image), obtained for each measured window.

We have applied this methodology of Mitchell and co-workers to evaluate the orientation parameters for the data in Figure 13 and 14 and the results are shown in Table 2. The series of orientation parameters describe the amplitudes of a series of spherical harmonics which describe the orientation distribution function D(α). These values, and higher order values where required, can be used to recreate the orientational distribution function for the normals to the chain folder lamellar crystals. For highly aligned systems probably the first 11 or 12 orientation parameters are required but for more intermediate levels of orientation probably 5 parameters will suffice. Figure 16 shows a plot in polar coordinates which shows the amplitudes of the function $P_{2n}(\cos\alpha)$. These are normalised amplitudes which range from 1, for a orientation distribution function with all of the structural units with a common alignment to 0 for an isotropic distribution where all alignments are equally possible. These parameters can be calculated as a function of time for a fixed sampling position, or as a function of position as shown in Figures 13 and 14. The curves shown in these Figures underlines the importance of the alignment of the injection moulding system on the beamline. For these data, window 1 was aligned so as to position the incident beam in the centre of the window and then we used the information of the positions of the other windows from the matching process. In future work we will perform the alignment of each window on an individual basis and use the translation stages to move to each defined position based on the alignment.

Preprints (www.preprints.org) | NOT PEER-REVIEWED | Posted: 15 August 2023 doi:10.20944/preprints202308.1135.v1

Table 2. Orientation Parameters describing the level of preferred orientation for PP1 and PP2 based on the data shown in Figures 13 and 14 for window 1

D_{2n}	PP1	PP2
D_2		0.50
D_4		-0.28
D_6		-0.26

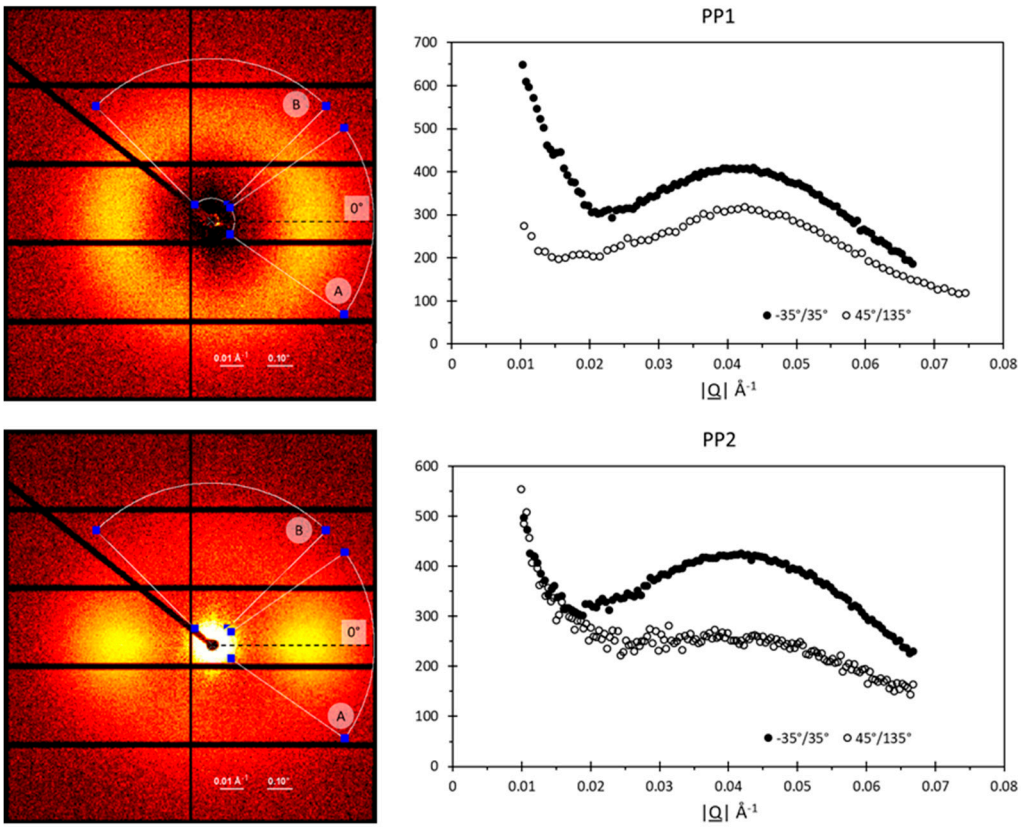

Figure 15. Radial integration over a selected range of a angles. Left diagrams visualize a schematic representation of the azimuthal integration ranges superimposed on the SAXS pattern which the integration was applied, being A the range -30°/30° and B 45°/135°. On the right are shown the resulting profiles of the integration. Top images correspond to PP1 while PP2 results are in the bottom line.

Figure 15 shows the results of integrating the data over a specific azimuthual range to enhance the signal to noise ratio, as the random fluctuations about a mean value inherent in a photon counting systems rapidly cancel out. The differences in the resultant curves shown in Figure 15 reflect the different level of anisotropy present in these two samples. In Table 3 are reported the calculated long period Lp values (see section 3.1) for the profiles in Figure 15.

Table 3. Lp values for the selected profiles integrated over specific angles.

Lp (Å)	PP1	PP2
-35°/35°	113	106
45°/135°	121	116

Preprints (www.preprints.org) | NOT PEER-REVIEWED | Posted: 15 August 2023 doi:10.20944/preprints202308.1135.v1

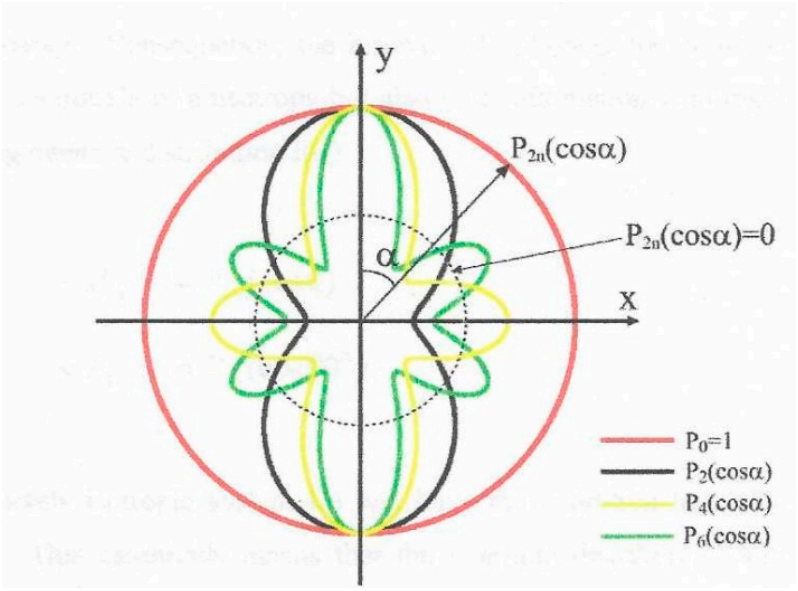

Figure 16. Plots of the first four Legendre Polynomials used in the work, plotted in polar coordinates reproduced with permission from [31]

4.0. Discussion

The data shown in section 3 underlines the variety of data available and its quantiative nature. It is possible to obtain adequate quality SAXS patterns in 1s and use these to follow the arrival of the molten plastic in the mould cavity and subsequely follow its transformation to a semi-crystalline solid. We are able to observe variations in the temperature of the plastic through the change in the long period peak position. We are able to quantitatively evaluate the level of preferred orientation of the lamellar chain folded crystals which form as a function of time. Through simple and rigorous manipulation of the data we are able to follow the development of the morphology beyond the first second. The flexibility of the mould design means that it is straightforward to design and implement new mould cavities to evaluate specific aspects of the injection moulding process. In some cases, this will involve replacement of the mould inserts and in others, the mould plates will also need changing. Since these are all standard components, the resources required to perform these experiments will be minimised. Although the work reported here was focused on standard isotactic polypropylene resins, the injection unit has an upper temperature of 420 °C, and so a much wider range of materials can be studied. The mould temperature is maintained using two industrial recirculation units and a switch to enable both heating and colling modes. The full range of processing parameters can be varied. The injection unit is fitted with an Euromap interface which facilitates the addition of other components to the injection moulding systems. In future experiments we will be implementing the triggering of the injection moulding cycle by the hardware and software of the beam to start the moulding cycle after collecting 10 SAXS patterns. Other developments planned include the rapid heating of the mould using induction heating [32,33] and other methods. Future experiments will also include a wider range of materials including bioplastics such as polyhydroxybutyrate and polybutylene succinate.

In these first validating experiments we have settled on a time step of 1s. This allows 10 SAXS patterns to be recorded in the early stage of the injection moulding cycle (Figure 6). Now clearly it would be advantageous to decrease this time period, say to 0.5s or even 0.2s. Of course, the more patterns recorded, the more time is lost in resetting the detector and storing the data. The transmission measurement used to provide a timing marker for the arrival of the plastic in the mould cavity is also made in this 1s data accummulation cycle. There would be an advantage of measuring this at a high frequency, but this would involve modification to the beamline system and we will raise this if it becomes pressing requirement.

 doi:10.20944/preprints202308.1135.v1

Reducing the time step for the data accummulation stage requires an increase in the brightness of the beamline. The source of the X-rays on the NCD-SWEET beam is a vacuum undulator and is already one of the brightest sources available. ALBA has a development plan "ALBA -2" [34] which is focused on upgrading the ALBA Synchrotron Light Source from a 3rd generation source to a 4th generation source by greatly reducing the emittance of the storage ring. Undoubtably, the new facility will have a brighter NCD-SWEET beamline, the effectiveness of which will depend on many factors including the beamline optics and the detectors. . In the current configuration, the beamline can work from 6 keV to 20 keV but it is optimised between 8 keV and 15 keV where the best compromise between flux (2.0×10^{12} ph/s at 12.4 keV), beam size (110 x 110 μm^2 at 12.4 keV) and absorption is achieved. The undulator can go to 2 keV, but the remainder of the beam-line optics is not setup for this energy and the channel cut monochromator would need modification. Moreover , the absorption of the sample and any windows for this energy of photons will be huge and only few photons will be collected on the detectors.

There are a wide range of synchrotron light sources across Europe and around the world. These all have different characteristics and operate with different energies of X-ray photons. In the current configuration, there is a trade off between the brightness of the source and the signal which will be measured in the detector. On one hand increasing the energy of the incident photons will increase the transmission through the aluminium alloy windows. There are many advantages of X-ray scattering with high energy photons [35] but above an energy of 10^4 eV, the coherent scattering cross-sections falls more or less linearly with photon energy. As a consequence, although more photons will reach the sample through a higher transmission through the aluminium windows, few photons will be scattered to provide a signal at the detector. We are currently assessing the possibilities at alternative synchrotron light sources and we will make a quantitative evaulation of the advantages of doing so.

A more immediate option is changing the nature of the windows. We have made simulations of the injection moulding process and evaluated the injection pressure required. Using this pressure, we have evaluated the effect on the thinned aluminium alloy windows. The main effect is that when the plastic is injected the temperature of the window area increases more than the surrounding mould and as a consequence there is a small expansion of the height of the window area and it leaves an almost imperceptible mark on the moulded product [25]. Once the temperature reduced, the window area returns to its original form. We will explore such simulations if thinner windows are possible to provide a great transmission. Our current ambition is to maintain the industrial relevance of this injection moulding system and so we have set aside the possibility of preparing windows with less absorbing materials not least to avoid the problems of sealing the windows and creating gradients of thermal conductivity.

5.0. Summary

1. We have successful developed and tested operando X-ray scattering measurements during injection moulding. We are able to obtain useful quantitative data on the rate of crystallisation, local temperature variations and the pattern of preferred orientation of the lamellar crystals.
2. We are able to operate on a 1s data cycle time and the possibilities of reducing this to 0.5s are promising.
3. The design of the injection moulding unit enables modifications to be made easily and control the processing parameter.
4. On this basis of these validation experiments, we are posied to perform defined injection moulding cycles to test specific aspects of the process of transforming molten plastic in to a shaped moulded solid product.
5. These validation experiments have confirmed that the microscopic characteristics of the process of transforming molten plastic to solid plastic are reproducible with successive moulding cycles, and this opens up the possibility of exploring spatial variations within the mould cavity using the predetermined window locations.
6. We have been able to obtain quantitative time-resolving data which can be compared with the predicts of computer simulations.

Author Contributions: For research articles with several authors, a short paragraph specifying their individual contributions must be provided. The following statements should be used "Conceptualization, X.X. and Y.Y.; methodology, X.X.; software, X.X.; validation, X.X., Y.Y. and Z.Z.; formal analysis, X.X.; investigation, X.X.; resources, X.X.; data curation, X.X.; writing—original draft preparation, X.X.; writing—review and editing, X.X.; visualization, X.X.; supervision, X.X.; project administration, X.X.; funding acquisition, Y.Y. All authors have read and agreed to the published version of the manuscript." Please turn to the CRediT taxonomy for the term explanation. Authorship must be limited to those who have contributed substantially to the work reported.

Funding: This work was financially supported by the *Fundação para a Ciência e a Tecnologia* FCT/MCTES (PIDDAC) through the following Projects: MIT-EXPL/TDI/0044/2021, UIDB/04044/2020; UIDP/04044/2020; Associate Laboratory ARISE LA/P/0112/2020; PAMI - ROTEIRO/0328/2013 (Nº 022158), plus *EcoPlast, Materiais compósitos eco-sustentáveis para substituição dos plásticos convencionais,* ref POCI-01-0247-FEDER-069002, and INNOV-AM funded by National Agency of Innovation. M.A. is grateful for the support received from the Spanish *Ministerio de Ciencia, Innovación y Universidades*, with the mobility program of the FPI-MIN 2019 grant.

Data Availability Statement: The data obtained using the facilities of the ALBA Synchrotron Light Source are subject to the Generic data management policy at ALBA CELLS as can be accessed at Microsoft Word - Data_policy_Alba_v1.2_2017.doc (cells.es). The experimental data identifiers are available from the corresponding author after the end of the embargo period.

Acknowledgments: The X-ray Scattering Data presented were obtained at the ALBA synchrotron light source in Barcelona in collaboration with ALBA Staff.

Conflicts of Interest: The authors declare no conflict of interest.

References

1. Ebnesajjad, S. (2003) "Injection Moulding" Chapter 7 in "Melt Processible Fluoroplastics", Editor Sina Ebnesajjad pages 151-193 William Andrew Publishing, Norwich. ISBN 13: 9781884207969
2. Smith Hyatt and John W. Hyatt "Improvement in processes and apparatus for manufacturing pyroxyline" US Patent 133, 229. November 19, 1872.
3. Mitchell, P., Editor "Tool and Manufacturing Engineers Handbook: Plastic Part Manufacturing", Society of Manufacturing Engineers, 1996 online https://books.google.pt/books?id=Q4X1ovFVBvoC&printsec=frontcover&hl=pt-PT&source=gbs_ge_summary_r&cad=0#v=onepage&q&f=false accessed 30 July 2023
4. Sailors, H.R. & Hogan, J.P. (1981) History of Polyolefins, Journal of Macromolecular Science: Part A Chemistry, 15:7, 1377-1402. https://doi.org/10.1080/00222338108056789.
5. Mandelkern, L. *The Relation between Structure and Properties of Crystalline Polymers*. Polym J 17, 337–350 **1985**. https://doi.org/10.1295/polymj.17.337.
6. Hu, A.O., Hua, W-Q., Zhong, G.J., Wang, Y-D., Gao, Y-T., Hong, C-X., Li, Z-M., Bian, F-G., Xiao, T-Q., Macromolecules 2020, 53, 15, 6498–6509. https://doi.org/10.1021/acs.macromol.0c01177
7. Björn, L., Mazza, R.M., Andreasson, E., Linell, F., Lutz-Bueno, V., Guizar-Sicairos, M., Jutemar, E.P., and Liebi, M. ACS Appl. Polym. Mater. 2023, XXXX, XXX, XXX-XXX
8. Michael J. Elwell, Mortimer, S., and Ryan, A.J., "A Synchrotron SAXS Study of Structure Development Kinetics during the Reactive Processing of Flexible Polyurethane Foam "Macromolecules 1994, 27, 19, 5428–5439. https://doi.org/10.1021/ma00097a024
9. J.L. Stanford, J.R. Powell, A.N. Wilkinson, "Structural composites formed by reaction injection moulding", in Editor(s): A G Gibson, FRC 2000–Composites for the Millennium, Woodhead Publishing, 2000,191-199, ISBN 9781855735507, https://doi.org/10.1533/9780857093134.191
10. Mateus, A,, Bartolo, P., and Mitchell, G.R.,"In-situ time-resolving small-angle X-ray scattering studies of reaction kinetics and morphology in reaction injection moulding" unpublished work
11. R. Kolb, S. Seifert, N. Stribeck, H.G. Zachmann, "Investigation of the high-speed spinning process of poly(ethylene terephthalate) by means of synchrotron X-ray diffraction" Polymer, 41, 2000, 2931-2935, https://doi.org/10.1016/S0032-3861(99)00463-2
12. van Drongelen, M., Cavallo, D., Balzano, L., Portale, G., Vittorias, I., Bras, W., Alfonso, G.C. and Peters, G.W.M. (2014), Structure Development of Low-Density Polyethylenes During Film Blowing: A Real-Time Wide-Angle X-ray Diffraction Study. Macromol. Mater. Eng., 299: 1494-1512. https://doi.org/10.1002/mame.201400161
13. E.M. Troisi, M. van Drongelen, H.J.M. Caelers, G. Portale, G.W.M. Peters, Structure evolution during film blowing: An experimental study using in-situ small angle X-ray scattering, European Polymer Journal 74, 2016, 190-208, https://doi.org/10.1016/j.eurpolymj.2015.11.022
14. Qianlei Zhang, Wei Chen, Haoyuan Zhao, Youxin Ji, Lingpu Meng, Daoliang Wang, Liangbin Li, "In-situ tracking polymer crystallization during film blowing by synchrotron radiation X-ray scattering: The critical role of network", Polymer, 198 2020, 122492, https://doi.org/10.1016/j.polymer.2020.122492

15. Li, YW., Liu, GF., Wu, HJ. et al. BL19U2: Small-angle X-ray scattering beamline for biological macromolecules in solution at SSRF. NUCL SCI TECH 31, 117 (2020). https://doi.org/10.1007/s41365-020-00825-3
16. Tao Liao, Xintong Zhao, Xiao Yang, Phil Coates, Ben Whiteside, David Barker, Glen Thompson, Yuqing Lai, Zhiyong Jiang, Yongfeng Men,"In situ synchrotron small angle X-ray scattering investigation of structural formation of polyethylene upon micro-injection molding", Polymer, 215, 2021, 123390, https://doi.org/10.1016/j.polymer.2021.123390
17. Costa, A.A.; Gameiro, F.; Potêncio, A.; Silva, D.P.d.; Carreira, P.; Martinez, J.C.; Pascoal-Faria, P.; Mateus, A.; Mitchell, G.R. Evaluating the Injection Moulding of Plastic Parts Using In Situ Time-Resolved Small-Angle X-ray Scattering Techniques. Polymers **2022**, 14, 4745. https://doi.org/10.3390/polym14214745
18. J.B. González*, N. González, C. Colldelram, L. Ribó, A. Fontserè, G. Jover -Manas, J. Villanueva, M. Llonch, G. Peña, A. Gevorgyan, Y. Nikitin, J.C. Martínez, C. Kamma-Lorger, E. Solano, I. Sics, S. Ferrer, M. Malfois 2018 Mechanical Eng. Design of Synchrotron Radiation Equipment and Instrumentation MEDSI2018, Paris, France JACoW Publishing ISBN: 978-3-95450-207-3 https://doi:10.18429/JACoW-MEDSI2018-THPH17
19. Ishige, R. Precise structural analysis of polymer materials using synchrotron X-ray scattering and spectroscopic methods. Polym J 52, 1013–1026 (2020). https://doi.org/10.1038/s41428-020-03572_
20. Saeed Mohan, Robert H Olley, Alun S Vaughan and Geoffrey R Mitchell 'Evaluating Scales of Structure in Polymers' in "Controlling Controlling the Morphology of Polymers: Multiple Scales of Structure and Processing." Springer 2016 ed G.R.Mitchell and A.Tojeira ISBN 978-3-319-39320-9
21. Shin, S. New era of synchrotron radiation: fourth-generation storage ring. AAPPS Bull. 31, 21 (2021). https://doi.org/10.1007/s43673-021-00021-4
22. D.H. Bilderback, B.W. Batterman, M. J. Bedzyk.K. Finkelstein, C. Henderson, A. Merlini.W. Schildkamp, Q. Shen, J. White, Blum, E.B., P.J. Viccaro, D. M. Mills, S. Kim, G. K. Shenoy, K. E. Robinson, F. E. James, and J.M. Slater (1989) "Performance of a hard X-ray undulator at CHESS" Rev. Sci. Instrum. 60 (7), 1419-1425
23. 6082 Aluminum Alloy 6082-T6 T651 AlMgSi1 (AlSi1MgMn - 3.2315) Properties (theworldmaterial.com) online accessed 30 July 2023
24. UAI - Babyplast online accessed 30 July 2023
25. Costa, A.A., Gameiro, F., Olivereria, L., da Silva, D.P., Carreira, P., Martínez, J.C., Martinho, P.G., Mateus, A., Mitchell, G.R., "Industrially relevant Injection Moulding Apparatus for Operando Time-Resolving Small-Angle X-ray Scattering Measurements" J. Manufacturing Processes submitted
26. Keller, A., & Kolnaar, HWH. (1997). Flow-induced orientation and structure formation. In Materials Science and Technology (pp. 187 - 268).
27. Pinheiro J., Abdulghani, S., Pascoal-Faria, P., Sousa, D., Pedro Carreira, Tânia Viana, Christina S. Kamma-Lorger, Geoffrey Mitchell; Tools to define and evaluate morphology mapping, a route to complex structures using direct digital manufacturing. AIP Conference Proceedings 24 July 2019; 2116 (1): 230003. https://doi.org/10.1063/1.5114229
28. Lovell, R. & Mitchell, G. R. (1981). Molecular orientation distribution derived from an arbitrary reflection. Acta Cryst. A37, 135–137.
29. Mitchell, G.R., Saengsuwan, S., Bualek-Limcharoen, S. (2005). Evaluation of preferred orientation in multi-component polymer systems using X-ray scattering procedures. In: Stribeck, N., Smarsly, B. (eds) Scattering Methods and the Properties of Polymer Materials. Progress in Colloid and Polymer Science, vol 130. Springer, Berlin, Heidelberg.
30. L. Hay, M. Jaffe & K. F. Wissbrun (1976) A phenomenological model for row nucleation in polymers, Journal of Macromolecular Science, Part B, 12:3, 423-428, https://doi.org/10.1080/00222347608019329
31. James J Holt, Supatra Pratumshat, Paula Pascoal-Faria, Artur Mateus, and Geoffrey Robert Mitchell "Crystallisation from Anisotropic Polymer Melts" Chapter 10 in "Polymer crystallization: Methods, Characterization, and Applications", editors Jyotishkumar Parameswaranpillai, Jenny Jacob, Senthilkumar Krishnasamy, Aswathy Jayakumar, and Nishar Hameed Wiley-VCH 2023 pages 225-284 ISBN 9783527350810
32. Muszyński, Paweł, Przemysław Poszwa, Krzysztof Mrozek, Michał Zielinski, Piotr Dalewski, and Michał Kowal. 2021. "Design and Simulation Study of the Induction Heated Injection Mold with Sliders" Materials 14, no. 23: 7476. https://doi.org/10.3390/ma14237476
33. R. Sánchez, A. Martinez, D. Mercado, A. Carbonel, J. Aisa, (2021) "Rapid heating injection moulding: An experimental surface temperature study",Polymer Testing, 93, 106928, https://doi.org/10.1016/j.polymertesting.2020.106928
34. ALBA II — en (albasynchrotron.es) ONLINE accessed 30th July 2023
35. Reichert, H., Honkimäki, V. (2015). High-Energy X-ray Scattering and Imaging. In: Jaeschke, E., Khan, S., Schneider, J., Hastings, J. (eds) Synchrotron Light Sources and Free-Electron Lasers. Springer, Cham. https://doi.org/10.1007/978-3-319-04507-8_33-1.